学位論文（部分公表版）

Synthesis, crystal structure, and first-principles calculations of a cyanide-bridged copper-molybdate bimetallic assembly

（銅－オクタシアノモリブデン錯体の合成、結晶構造、および第一原理計算）

平成２７年１２月博士（理学）申請

東京大学大学院理学系研究科

化学専攻

梅田　喜一

Abstract

Molecular magnetism has been studied as an interdisciplinary theme on the border of chemistry, materials science, and physics. In this area, control of physical properties by external stimuli is aggressively studied as an important target. Photomagnetism, control of magnetic properties by light irradiation, is attracting attention due to its potential toward applications in information storage and processing. Among photomagnetic materials, bimetallic copper octacyanidomolybdate with the general formula of $Cu^{II}_2[Mo^{IV}(CN)_8]\cdot nH_2O$ is known as a classical photo magnet, for which our group firstly reported photo-induced reversible magnetization with a Curie temperature of 30 K in 2001. After the report, various copper octacyanidomolybdate bimetal assemblies have been studied as photoresponsive magnetic materials. The mechanism of photomagnetism has been considered as the metal to metal charge transfer from Mo^{IV} (S = 0) to Cu^{II} (S = 1/2). The charge transfer produces Mo^{V} (S = 1/2) and Cu^{I} (S = 0), while the other Cu^{II} centers remain due to 2:1 Cu/Mo stoichiometry. The ferromagnetic interaction between S = 1/2 spins of Cu^{II} and Mo^{V} has been considered to be the origin of photomagnetism. However, the mechanism of photomagnetism in copper octacyanidomolybdate is the issue under discussions due to absence of the precise structural analysis for $Cu^{II}_2[Mo^{IV}(CN)_8]\cdot nH_2O$. There are some efforts to reveal the structure, and it was estimated to be the analogous of $M^{II}_2[Mo^{IV}(CN)_8]\cdot nH_2O$ (M^{II} = Mn^{II}, Fe^{II}, and Co^{II}) assemblies with tetragonal crystal system by wide-angle X-ray analysis and X-ray absorption spectroscopic analysis. As the structure is highly symmetrical and simple, it is expected to be a suitable model for calculations to examine the mechanism of photomagnetism. However, due to its poor crystallinity, a single crystal X-ray analysis was unavailable, and desired for further studies. In this study, the synthesis towards the single crystals, crystal structure, and first-principles calculations by a GGA + U method of a copper(II) octacyanidomolybdate(IV) bimetallic assembly $\{[Cu^{II}(H_2O)]_2[Mo^{IV}(CN)_8]\}\cdot 2H_2O$ (**CuMo**) are reported.

Synthesis and characterization

A single-crystalline form of the target material was obtained by using a gel method. The gel was obtained by mixing a portion of $Na_2SiO_3 \cdot 9H_2O$, acetic acid, and $K_4[Mo^{IV}(CN)_8] \cdot 2H_2O$ powder. The aqueous solution of $Cu(NO)_3 \cdot 3H_2O$ was added on the top of the gel. After the system was kept in dark for ca. 6 months, black block crystals were obtained. The elemental analyses by inductively coupled plasma mass spectrometer, a standard micro-analytical method, and a thermo-gravimetrical (TG) measurement confirmed that the formula is $Cu_2MoC_8H_8N_8O_4$. Calcd. Cu: 25.3%; Mo: 19.1%; C: 19.1%; H: 1.6%; N: 22.3%. Found Cu: 25.3%; Mo: 19.0%; C: 19.2%; H: 1.7%; N: 22.5%. The TG measurement shows two steps of weight loss in the range of 30−40 (step 1) and 120−130 ^oC (step 2). The weight loss of both steps are about 7.2%. Steps 1 and 2 correspond to desorption of coordinated and non-coordinated water, respectively. The infrared spectrum showed two peaks due to cyanide stretching vibration modes at 2185 and 2167 cm^{-1}.

Crystal structure

The single crystal X-ray diffraction analysis revealed that **CuMo** has tetragonal *I*4/*mcm* space group with the lattice constants of a = 11.2833(6) Å, c = 12.8491(8) Å. **CuMo** possesses a three-dimensional network structure, in which Cu^{II} and Mo^{IV} centers are alternately bridged by cyanide. The skeleton of the cyanido-bridged network is an analogue of other 3d transition metal assemblies, $\{[M^{II}(H_2O)_2]_2[Mo^{IV}(CN)_8] \cdot nH_2O$ (M^{II} = Mn^{II}, Fe^{II}, and Co^{II}). **CuMo** shows a tetragonal crystal system with unit cell parameters similar to the analogues. However, **CuMo** reveals higher symmetry and fewer coordinated waters than that of the analogues. The independent unit consists of one Cu^{II} center and one Mo^{IV} center. The coordination geometry of Mo^{IV} center is 8-coordinated square antiprism (D_{4d}), which is the highest symmetry for 8-coordinate centers. The coordination geometry of Cu^{II} center is 5-coordinated square pyramid. The equatorial positions of the square pyramid are occupied by four nitrogen atoms from bridging cyanides, and the axial position is occupied by one oxygen atom from coordinated water. The position of the coordinated water is disordered into two positions with the occupancy

of 50%. The non-coordinated water molecules are located in the structural pores along *c* axis. Coordinated and non-coordinated water molecules are forming hydrogen bonding network extending along *c* axis. The crystal structure of **CuMo** is stabilized by both the hydrogen bonding and cyanide bridging.

First-principles band calculations

The first-principles calculations were conducted by using Vienna ab initio simulation package (VASP) with a GGA + *U* method. Structural optimization from the result of the single crystal X-ray diffraction analysis as the initial structure was applied. **CuMo** reveals a direct optical transition at the Γ point with a band gap of 1.2 eV. The conduction bands above 1.0 eV are occupied by two Mo^{IV} 4d-based bands. Although these bands show energy splitting, the charge density of these bands are very similar. This splitting can be attributed to a difference in phases of the atomic orbitals for equivalent atoms in the calculated primitive unit cell. The valence bands below 1.8 eV are occupied by two Cu^{II} 3d-based bands. The energy splitting between the same spins is originated from the difference in phase like for the valence bands. In addition, the splitting between the different spins are caused by the difference of coordination geometry due to the disordered coordinated waters. The valence bands in the range of −2.0 to −1.0 eV consist of the oxygen 2p-based bands from the non-coordinated water. The conduction bands above 1.8 eV are composed of the carbon and nitrogen atoms of cyanide ligands with a slight contribution from Mo^{IV}. As a result of an absorption spectrum calculation, the optical transition between the highest valence band and the lowest conduction band are found to be the main contribution to absorption in the visible range. The direction dependence of absorption strength indicates the strongest absorption along [1 1 1] crystallographic direction, where the cyanide ligands are aligned in parallel. The highest valence band consists of Mo^{IV} d_{z^2} orbital and nitrogen p_z orbital, while the lowest conduction band is composed of Cu^{II} $d_{x^2-y^2}$ orbital, nitrogen sp_x orbital, and carbon sp_x orbital. Among these bands, orbital overlap exists only around the nitrogen center. The transition of $p_z \rightarrow sp_x$ of nitrogen gives the strong transition moment due to the orbital difference in the orbital angular momentum and parity. This result confirms the charge

transfer from Mo^{IV} to Cu^{II} is realized through the transition moment on nitrogen atom of cyanide ligand, which results also in the anisotropy of the optical transition.

Conclusions

In this work, the single crystalline form of a three-dimensional copper(II) octacyanido-molybdate(IV) was successfully synthesized, and the crystal structure was determined. The crystal structure is a tetragonal three-dimensional network structure similar to analogues with other 3d transition metals. Using the experimentally determined crystal structure, first principles calculations with a GGA + *U* method were performed. **CuMo** shows a direct transition at the Γ point with a band gap of 1.2 eV, and the optical transitions in the visible range were assigned to the charge transfer from Mo^{IV} to Cu^{II}. The absorption strength analysis suggests the anisotropic absorption along [1 1 1] crystallographic axis, which is parallel to the arrangement of cyanides. In addition, as the result of the charge density analysis, the charge transfer between Mo^{IV} and Cu^{II} in the visible range was found to be facilitated by the optical transition of nitrogen from bridging cyanides, i.e. the changes of the parity and the symmetry caused by the $p_z \rightarrow sp_x$ transition of nitrogen enable the efficient charge transfer. The results in this work are expected to give a design criteria for new functional copper octacyanidomolybdate-based and other related photomagnetic materials.

Index

Chapter 1.

Introduction

1.1. Photo responsive material

External field responsive materials are studied due to their potential towards application in sensors and memories. For example as the external stimuli, light, pressure, electric field, magnetic field, and humidity can be applied. Among them, the photo-responsive materials are studied towards its application for optical recording media and information processing. Since a long time, inorganic salts (e.g. silver halides) are used for photosensitizer dyes of photographs. The other practical photo responsive materials are photochromic molecules which show reversible switching between two colors by light irradiation. Azobenzenes, cyanine, and phthalocyanine are used as practical recording media of rewritable optical discs. [1] However, their weak point is a low cycle durability. In recent years, highly durable photochromic molecules (e.g. diarylethenes) have been developed as a target of this research field. [2, 3] In the field of coordination chemistry, some spin crossover molecules have been studied as photochromic molecules, and the related phenomena is called light induced excited spin state trapping (LIESST). [4−6]

Recently, chalcogenides (e.g. GeSbTe and AgInSbTe) are utilized for rewritable high density optical media such as DVD and Blu-ray discs. Chalcogenides are used in so called phase change memories. [7] Phase change memory realizes two different state by the two separated phases. For example, chalcogenide shows two different phases in room temperature after heating, which are amorphous phase by rapid-cooling and crystal phase by slow-cooling, and they show different reflectance values. Their merit in contrast with the photochromic molecules is threshold of their phase transition. Simple photoreaction is promoted with no energy density dependency. Therefore, undesired photo reactions occur by weak ambient light, and the effect spoils durability. On the other hand, if light below the threshold energy density is irradiated, phase change does not occur.

In the area of organic molecular substances, photo-induced neutral-ionic transition was

reported for tetratiafuluvalen-chrolanil (TTF-CA). [8] In the area of metal complexes, the cooperative LIESST effects have been studied, and the phase transition at room temperature was observed in a spin crossover complex, Fe(pyrazine)[Pt(CN)$_4$]. [6] Lately, our group reported the first example of a metal oxide exhibiting room temperature photo-induced reversible phase transition material λ-Ti_3O_5. [9] This material is transformed to β-Ti_3O_5 by a green pulse laser irradiation and returns to λ-Ti_3O_5 by a blue continuous laser irradiation. Moreover, our group recently reported that the pressure-induced phase transition from λ-Ti_3O_5 to β-Ti_3O_5 is also possible. [10] This material is a simple titanium oxide, which exists in a large amount in earth and it is harmless. Above all, as this transition process requires no thermal time course control, the switching can be realized by a simple device with rapid response.

In addition, control of physical properties by external stimuli are aggressively studied as an interdisciplinary area between chemistry, physics, and material sciences. [11] Conjunction of external stimuli responsivity and physical properties such as ferromagnetism, ferroelectricity, electric conductivity, and ion conductivity are studied for their unique functionality. These physical properties cause as macroscopic effects in materials, and they are expected to show huge observable response applicable to towards new functional devices.

1.2. Cyano-bridged bimetallic assembly

Molecular-based magnets are studied owing to their high designability and fascinate functionalities. [11−18] Cyano-bridged bimetallic assemblies are classified as a family of molecular-based magnets and studied due to its attractive characteristics such as photo-sensitivity, magnetic interactions, flexible structure, and various coordination geometries, which lead to external stimuli responsive physical properties.

Cyanide bridged bimetal assemblies are consisted of two metal ions (*M* and *M*′), which are alternately bridged by cyanide ligands (−*M*−CN−*M*′−). In the polycyanidometallate-based systems, various metal cations and coordination numbers are possible. For example, six, seven, and eight coordinated polycyanidometallate can be used as building blocks. Moreover, organic

ligands can be additionally introduced. As the result of such a high designability, a lot of cyanido-bridged functional materials are synthesized.

Hexacyanidometallate

The well-known hexacyanometallate-based material is a Prussian blue $Fe^{III}_4[Fe^{II}(CN)_6]_3 \cdot 7.5H_2O$. This compound shows vivid blue color due to its mixed valence character originating from the presence of Fe^{II} and Fe^{III}. [19] The analogues with substituted transition metal ions and introduced alkaline cations are called Prussian blue analogues (PBAs). The most of PBAs consist of two types of transition metal cations: a divalent metal cation (M_A^{II}) and a hexacyanometallate anion containing trivalent cation (M_B^{III}) (Figure 1.1). They reveal rigid jungle-gym-type three-dimensional network structure (Figure 1.2). To ensure charge neutrality, two general forms of PBAs are formed. The first is a vacant type with the general formula of $M_A^{II}[M_B^{III}(CN)_6]_{2/3} \cdot nH_2O$ which adopts centrosymmetric *Fm*-3*m* space group. [20] The other one is a non-vacant type with the general formula of $A^I M_A^{II}[M_B^{III}(CN)_6]_{2/3} \cdot nH_2O$ (A^I: monovalent alkaline cation) which takes non-centrosymmetric *F*-43*m* space group. [21] The PBAs have been studied as electrode materials [22–24], porous materials [24–26], and magnetic materials [26–37]. As the electrode material, the alkaline cation input-output characteristics are studied aiming at the application for a cathode material of a battery. [24] As a porous material, the absorption property of PBAs arouse a considerable attention such as the gas and alkaline cation absorption could be observed. [24–26] As a magnetic material, various novel phenomena have been investigated. High Curie temperatures are observed for molecular magnets in a Cr-based PBA (in 1993, T_c = 240 K) [28] and a V-Cr assembly (in 1995, T_c = 315 K). [29] In this context, our group reported ferro-ferri mixed magnetism, [30,31] photo-induced magnetic polar inversion, [32] humidity sensitive magnetism,[26] coexistence of ferroelectricity and ferromagnetism, [33] photo-induced phase collapse,[34] coexistence of ferromagnetism and ion conductivity, [35] and others. The important point is that these functionality can be designed by metal cations and molecular magnetism theory due to the rigid skeleton of PBAs which is retained after metals are substituted. [36,37]

Octacyanidometallate

Among the cyano-bridged bimetallic assemblies, eight coordinated building block, octacyanidometallate can form various network structures due to various coordination geometries of square-antiprism, dodecahedron, and bicapped trigonal prism. Their similar energy levels result in the absence of specific preferable coordination geometry (Figure 1.3). Octacyanidometallates form network structure with transition metal cations in the similar manner to hexacyainidometallates. Mn^{II}, Co^{II}, Ni^{II}, Cu^{II}, Zn^{II} are applicable as transition metal cations *M*, and $Mo^{IV/V}$, $W^{IV/V}$, Nb^{IV}, Re^{V} are achievable to be a metal center of octacyanidometallates anions, $[M'(CN)_8]^{n-}$. In addition, organic ligands can be introduced. The cyanide bridged network topologies can be controlled reasonably by introducing organic ligands. [37] 0-D [38] (dimensional), 1-D [39], 2-D [40], 3-D [41] compounds have been prepared (Figure 1.4). Within this various structures, the correlation between the structure and the physical properties and their external stimuli response have been studied. Our group reported a high-spin cluster [42], photoinduced magnetization [43−52], meta-magnetism [53], chemical stimuli responsive magnet [54], magnetization-induced second harmonic generation (MSHG) [55], electric field-induced phase transition [56], and others. Among them, photomagnetism has been studied as the major functionality of these materials as described in the next section.

1.3. Photomagnetism in octacyanidometallates

Photomagnetism is studied due to its potential towards application in data storage and information processing. Our laboratory has reported some kinds of octacyanido-based photo magnets indicating, Cu-Mo (Figure 1.5) [43−46], Co-W (Figure 1.6) [47−50], and Fe-Nb (Figure 1.7) [51−52] bimetallic assemblies. All of them are non-magnetic phase before irradiating light. However, by light irradiation, spontaneous magnetization is induced, and they show ferromagnetic behavior. This phenomenon is called photo-induced magnetization. All these compounds reveal photo-induced magnetization. The photo-induced magnetization can turn off by the thermal annealing,

and some compounds show photo-reversibility. The mechanisms of photo-magnetism in octacyanidometallate can be classified into three types as follows.

Photo-induced charge transfer

The mechanism of photomagnetism in Cu-Mo bimetallic assemblies has been considered as the photo-induced metal-to-metal charge transfer. By irradiation using blue laser light, Mo^{V} (d^{1}, $S = 1/2$) and Cu^{I} (d^{10}, $S = 0$) are produced as a result of the photo-induced metal to metal charge transfer from Mo^{IV} (d^{2}, $S = 0$) to Cu^{II} (d^{9}, $S = 1/2$) while the other Cu^{II} centers remain due to 2:1 Cu/Mo stoichiometry. The ferromagnetic interaction between $S = 1/2$ spins of Cu^{II} and Mo^{V} has been considered to be the origin of photomagnetism. Additionally, a specific Cu^{II}-Mo^{IV} bimetallic assembliy (discussed in the next section) return to paramagnet by the red light irradiation. [46] The reversibility is explained by the reverse metal-to-metal charge transfer from Cu^{I} to Mo^{V}. The origin of this charge transfer was explained by mixed valency. In the class II of mixed valence compound in the Robin-Day classification[19], the energy barrier exists between the initial state and the photo-induced valence isomer state. The photo-induced valence isomer state can be stabilized by the energy barrier, and photo-induced magnetization is observed. However, other mechanism based on spin crossovers within Mo^{IV} centers ($S = 0 \rightarrow S = 1$) is also suggested as described later, and the reliability propriety of this mechanism is not obvious because this is not proved with explicit results. The photo-induced charge transfer can also be observed using the infrared spectra[57,58].

Charge transfer induced spin transition

The charge transfer induced spin transition (CTIST) is used for explanation of the photomagnetism in Co-W bimetallic assemblies. Before the light irradiation, this type of compounds adopt the diamagnetic electric configuration of low-spin (LS) Co^{III} (d^{6}, $S = 0$) and W^{IV} (d^{2}, $S = 0$). By light irradiation, the charge transfer from W^{IV} to Co^{III} is induced, and the intermediate state of LS Co^{II} (d^{7}, $S = 1/2$) and W^{V} (d^{1}, $S = 1/2$) is obtained. In this system, Co^{II}

prefers the high-spin (HS) state of Co^{II} (d^7, $S = 3/2$). Consequently, the photoinduced HS Co^{II} (d^7, $S = 3/2$) and W^{V} (d^1, $S = 1/2$) centers are produced, and ferromagnetic interaction between them result in the photo-induced magnetization. As the transformation between LS and HS accompanies large volume changes, the large cooperative effect exists between the same state centers. Thus, a highly stable bistability with a huge thermal hysteresis loop can be detected.

Light induced excited spin state trapping

The light induced excited spin state trapping (LIESST) is observed in Fe-Nb bimetallic assemblies. This kind of compounds reveals the ground state of LS Fe^{II} (d^6, $S = 0$) and Nb^{IV} (d^1, $S = 1/2$). By light irradiation, the LIESST effect is induced that is a spin transition from LS Fe^{II} to HS Fe^{II} (d^6, $S = 2$). By the ferrimagnetic interaction between HS Fe^{II} and Nb^{IV}, the photo-induced magnetization is realized. As the LIESST effect is sensitive to the ligand field of Fe^{II} centers, the appropriate organic ligand should be coordinated to Fe^{II}. Moreover, a strong magnetic interaction to induce ferromagnetic behavior is required. Although the concept of spin crossover magnet has been expected since a long ago, the first example of the LIESST magnet is reported in 2011 due to the difficulty for the presented two reasons. In the present, we can expect the spin transition behavior of Fe^{II} using the ligand field energy obtained by molecular orbital calculations to some extent.

1.4. Copper(II) octacyanido-molybdate(IV) bimetallic assembly

Within the hot research area of photomagnetism, I have studied a photo-induced charge transfer in Cu-Mo bimetallic assembly. Here, I will introduce the target material of this thesis which is Cu – Mo cyanide-bridged bimetal assembly.

Photo-induced charge transfer in solution

The photoreactivity of the octacyanomolybdate ion was firstly studied in solution state within the area of basic photochemistry.[59,60] A charge transfer phenomenon was later investigated on

the mixed solution with divalence copper cation.[61,62] Before the light irradiation, an ion pair of Cu^{II} / $[Mo^{IV}(CN)_8]^{4-}$ exists. By the light irradiation, a Cu^{I} / $[Mo^{V}(CN)_8]^{3-}$ ion pair is generated by the charge transfer. After the irradiation of lower energy light, the reverse charge transfer is induced with the return generation of the Cu^{II} / $[Mo^{IV}(CN)_8]^{4-}$.

Photo-induced magnetization in the precipitated Copper(II) octacyanido-molybdate(IV) material of Cu^{2+} and $[Mo^{IV}(CN)_8]^{4-}$

By the reaction of highly concentrated aqueous solutions of Cu^{2+} and $[Mo^{IV}(CN)_8]^{4-}$, a powder form of the copper(II) octacyanidomolybdate(IV) assembly, $Cu^{II}_2[Mo^{IV}(CN)_8]\cdot nH_2O$ was obtained. This compound was the first example of octacyanidometallate-based photomagnet, and received much attention as a photo-responsive material (Figure 1.8). Our group firstly reported this material in 2001. [43] In the same period, the essentially identical compound was reported by C. Mathoniére *et al.*, and the photomagnetic behavior was also investigated. [63]

Before light irradiation, this compound shows a paramagnetic behavior. By the blue light irradiation this compound shows ferromagnetic behavior with a Curie temperature of 30 K. However, by the successively red light irradiation with three different wavelengths, the ferromagnetic behavior can be turned off. It means that this compound completely return to a paramagnetic from a ferromagnetic state. A complete reversibility like this was novel. Since these reports, a lot of other Cu-Mo based compounds were synthesized, and the photo-magnetic effects were observed by many groups. [63−73]

Despite the long scientific history from 2001, some challenges on $Cu^{II}_2[Mo^{IV}(CN)_8]\cdot nH_2O$ still remain, and they are described as follows.

Structural study

Firstly, no crystalline form was reported. As the obtained samples of $Cu^{II}_2[Mo^{IV}(CN)_8]\cdot nH_2O$ were at a poorly crystalline form, the X-ray diffraction studies were unavailable. Using other X-ray methods of X-ray absorption fine structure (XAFS) and wide-angle X-ray scattering (WAXS)

analyses [46] suggested the approximate structure of $Cu^{II}_2[Mo^{IV}(CN)_8]\cdot nH_2O$ which is an analogoue to tetragonal three-dimensional cyanido-bridge $M^{II}[Mo^{IV}(CN)_8]\cdot nH_2O$ assemblies built of 3d transition metal cations (M^{II} = Mn^{II}, Fe^{II}, and Co^{II}) and an octacyanomolybdate(IV) anion (Figure 1.9−11). [75−77] However, more precise structural data was needed for the further studies of this compound.

Mechanism of photo-induced magnetization

Secondly, for this Cu-Mo photomagnetic system, the mechanism of the photoinduced effect was proposed to be based on photo-induced charge transfer between Cu^{II} and Mo^{IV} but could not be proved, and it is still under discussion. The mechanism of the photo-induced magnetization has been understood by the photo-induced charge transfer as I described above. However, in some copper(II) octacyanidomolybdate(IV) assemblies, the possibility of the photo-induced spin transition of $[Mo^{IV}(CN)_8]^{4-}$ ion from $S = 0$ to $S = 1$ has also been suggested as the explanation of photo-induced change of magnetic properties, recently. [71−74] Thus, more detailed studies are desired to prove the mechanism of photo-induced magnetization.

1.5. Crystallization technique

Reaction forming Cu-Mo bimetallic assembly

The target compound was synthesized by the reaction of Cu^{2+} and $[Mo^{IV}(CN)_8]^{4-}$ in aqueous solution by the reaction:

$$2Cu^{2+} + [Mo(CN)_8]^{4-} + nH_2O \rightarrow Cu_2[Mo(CN)_8]\cdot nH_2O$$

In general, to synthesize the single crystal with good quality, nucleation velocity should be slower than that of nuclear growth. To make such a condition, some approaches can be considered. For example, reaction in strongly diluted solution, reaction at high temperature, and gradual transfer of the reactants were considered. In this system, reaction in a diluted solution is not effective due to the high nucleation velocity. Reaction at high temperature (40 ^{o}C) was tried in our laboratory

in the past, but it results in the creation of a very different structure (Figure 1.12) [78] from the previously reported the copper(II) octacyanidomolybdate(IV) based photomagnet.

This is because the most thermodynamically stable structure at the reaction temperature is formed. As the amorphous samples of the copper(II) octacyanidomolybdate(IV) assembly were synthesized at room temperature, the difference in the reaction temperature could result in the single crystals with another thermodynamically stable structure. In this point, the reaction temperature should be the room temperature which is the same as the reaction of previously reported copper(II) octacyanidomolybdate(IV) assembly of the remarkable photomagnetic property.

Gel method

I adopted a gel method as the improved synthetic approach based on gradual transfer of the reactants. [79] In the gel method, a reactant is closed in a gel, and gradually transfer to the outside of the gel. This method can control both nucleation and nuclear growth velocity at room temperature.

This technique was utilized since the 19th century, and during the period of 1913-1926, studies about “Lisegang ring” in gels have been reported. [80] Lisegang ring is periodic precipitation generated by slow diffusion of reactants. In a context of crystal engineering, this method has been employed to obtain high quality and well-shaped crystals.

As the gel mediator in this method, a silicic acid gel and an agarose gel are applicable. The crystal growth can be controlled by tuning the gel mediator. Silicic acid gels are obtained by the mixture of silicic acid solution and carbonic acid near the isoelectric point of silicic acid. The disposition of gel can be controlled by some parameters in the reaction, for example, temperature, selection of carbonic acid, and concentration of solution. By selecting precise parameters, the selected crystal habit can be individually created. [79]

1.6. Points of view to electric structure of materials

Today's computational chemistry has been strongly developed. Using calculational methods, we can simulate and examine electric structures of materials. If the electric structure is obtained, we can perform further studies using theoretical method. Mainly, two points of view exists to treat the electric structure of materials, i.e., the molecular orbital theory and the band theory.

Molecular orbital theory

Molecular orbital theory is a description for discussing the electric structure of the materials by focusing on the molecular orbitals. In this approach, isolated model molecules are treated. In the field of chemistry, this picture is frequently applied and successful in describing the electric structure of materials in gas or liquid phase. However, the solid state substances are packed in crystal structure. If the molecules are well isolated without bond nor interaction between each other in solid phase, a cluster model cut out from the solid is applicable just as it is. However, compounds with periodic structure with bonds or interactions along some directions, the approximation should be applied. For example, a cluster is cut out and point charges are set to the terminal of the bonds.

Band theory

Band theory is a description for discussing the electric structure of solids frequently used in the field of physics. In this picture, wave functions and intrinsic energies of electrons are written as a function of *k*-points in reciprocal space (or *k*-vector in real space). This picture is based on the Bloch's theorem. [81] A wave function satisfying a Bloch theorem is called Bloch function and they are depicted by the equation: ($\psi_{\boldsymbol{k}}(\boldsymbol{r}) = e^{i\boldsymbol{k}\cdot\boldsymbol{r}}\, u_{\boldsymbol{k}}(\boldsymbol{r})$) which shows a necessary condition of the basis functions. A reciprocal space and a real space are connected by the Fourier transform. The periodical structure can be treated by Fourier transform. Thus, the band picture can treat periodic structure as it is unlike for the molecular picture. Moreover, we can obtain information of the bulk materials by the analysis of the band structure (*k*-point dependency of intrinsic energies). However,

the computational cost of a band calculation is relatively large in comparison to a molecular orbital calculation. Thus, the band calculation and molecular orbital calculations are complementary used depending on systems.

1.7. Basic theory and practical methods for calculating an electric structure

Some kinds of theoretical methods are applied as calculational methods such as molecular dynamics theory, molecular orbital theory, density functional theory, and Monte Carlo method. Among them, recently, a density functional theory is the most frequently used in both of computational chemistry and physics owing to its reasonable calculational cost and accuracy.

Density functional theory [82]

The first example of density functional theory for quantum systems is proposed by Thomas [83] and Fermi [84] in 1927. Their approximation were not accurate enough for precise calculations. However, the approach indicated the way in which density functional theory works. In 1964, Hohenberg and Kohn proposed an approach to formulate density functional theory as the exact theory of many-body systems by proving two theorems. [85] The first one is that the external potential is determined uniquely by the ground state density. The second one is that the ground-state energy is the global minimum of a universal functional for the energy in terms of the density, and the density that minimizes the functional is the exact ground state density. In 1965, Kohn and Sham proposed the approach to replace the original many-body problem by an auxiliary independent-particle problem. [86] This has led to very useful approximations used in the contemporary first-principles calculations. In the Kohn-Sham method, a practical exchange-correlation functional is important for accurate calculations. As the development of exchange-correlation functionals and improvement of high efficient computers are well succeeded, the density functional theory gained a major position on the first-principles calculations.

The other advantage on the density functional theory method is the presence of the charge density in the obtained result. By the analysis in the calculated charge density, we can examine

the electric structure from the view of the molecular orbital. In particular, during the optical transition process, the orbital conformation change gives not only quantitative but also qualitative information.

1.8. Objective

The objective in this work is the investigation of the visible-light induced magnetization mechanism of $Cu_2[Mo(CN)_8]\cdot nH_2O$ by first-principles calculations based on the experimentally determined structure. Firstly, I have undertaken the challenge of the preparation of a single crystalline form of $Cu^{II}_2[Mo^{IV}(CN)_8]\cdot nH_2O$ with a good quality enough to be solved its structure by a single X-ray diffraction analysis. Next, I have performed first-principle band calculation using the obtained crystal structure with a generalized gradient approximation with coulomb repulsion parameter (GGA + *U*) method, and I have revealed the optical properties with the mechanism of the photo-induced charge transfer process in details.

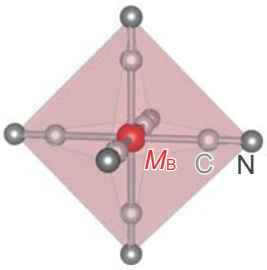

Figure 1.1. Coordination geometry of hexacyanidometalate.

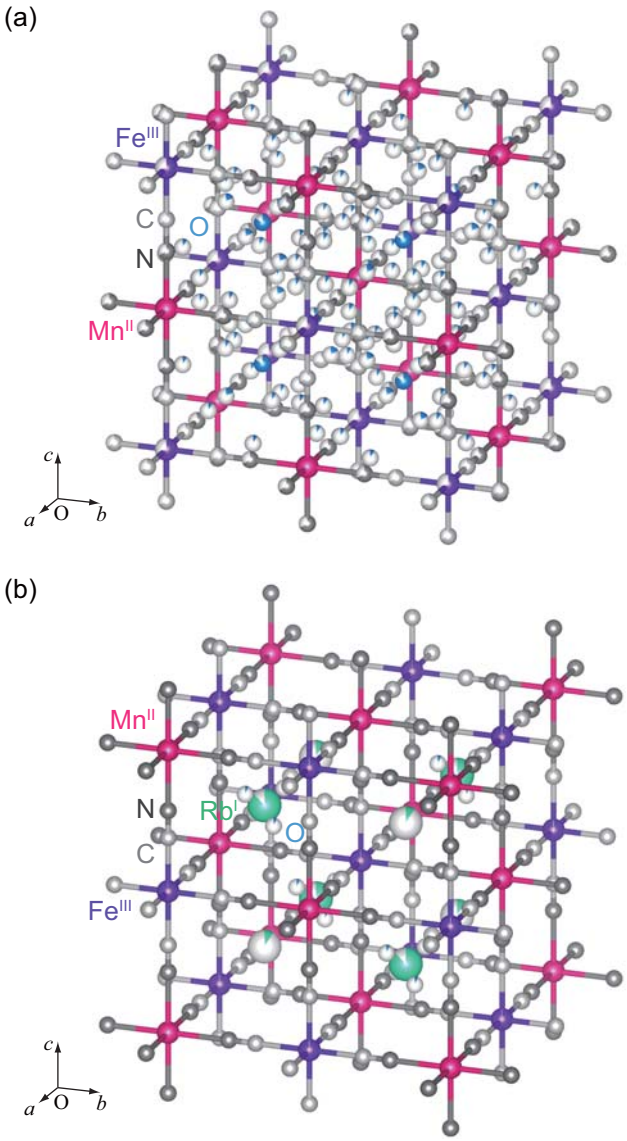

Figure 1.2. Crystal structure of Prussian blue analogues: (a) $M_A^{II}[M_B^{III}(CN)_6]_{2/3}\cdot 5H_2O$ with vacancies [20] and (b) $A^{I}M_A^{II}[M_B^{III}(CN)_6]_3$ with alkaline cations. [21]

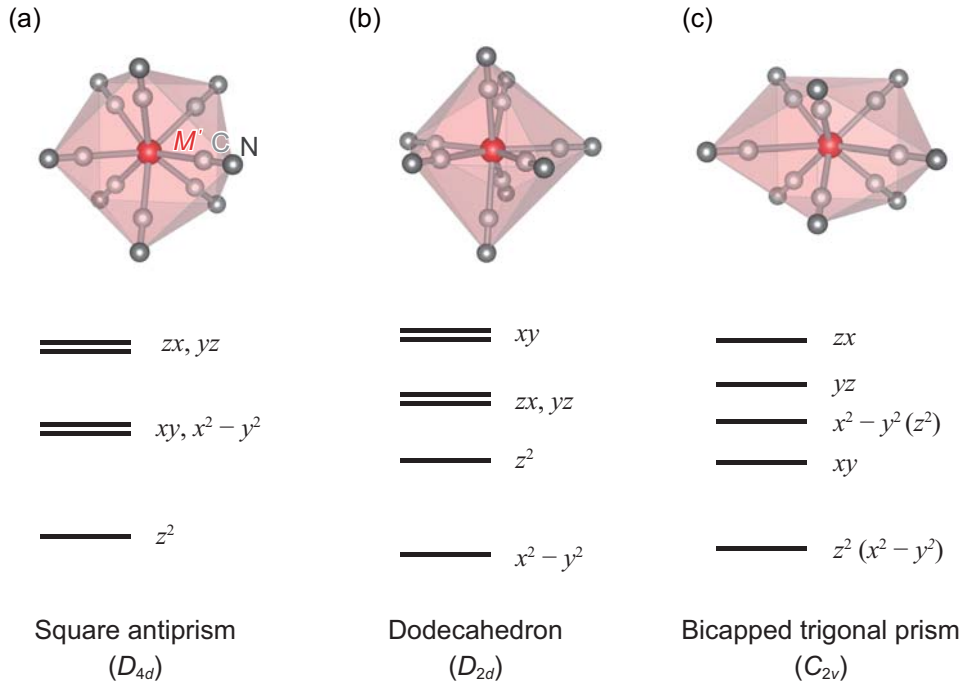

Figure 1.3. Coordination geometries and energy level diagrams of octacyanidometalate in the coordination geometry of (a) square antiprism, (b) dodecahedron, and (c) bicapped trigonal prism.

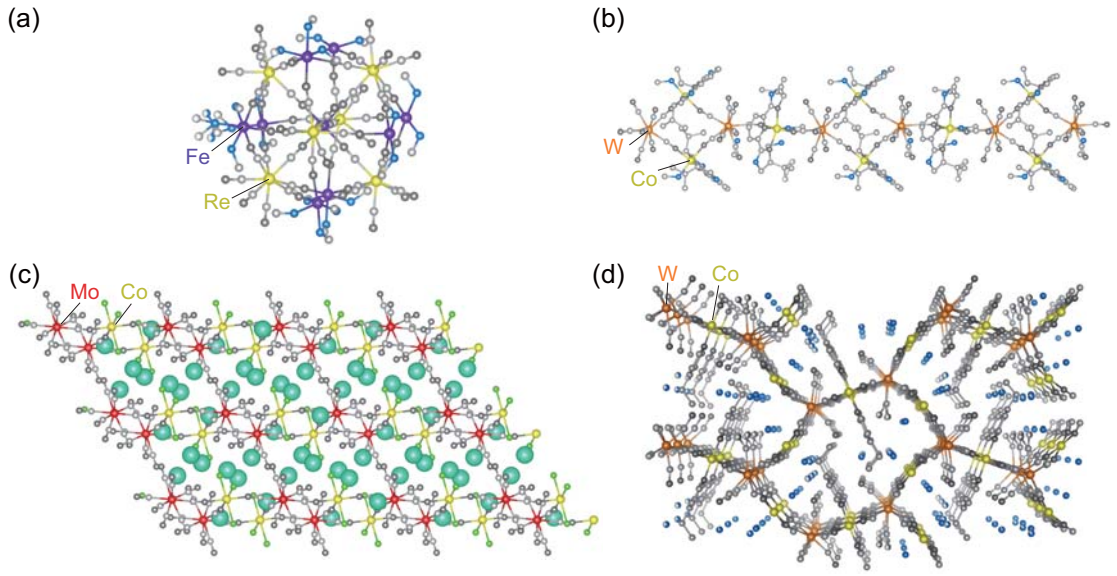

Figure 1.4. Crystal structure of octacyanidometallate based compounds: (a) a zero-dimensional Fe-Re based bimetallic assembly, [38] (b) a one-dimensional Co-W based bimetallic assembly, [39] (c) a two-dimensional Co-Mo based bimetallic assembly, [40] and (d) a three-dimensional Co-W based bimetallic assembly. [41]

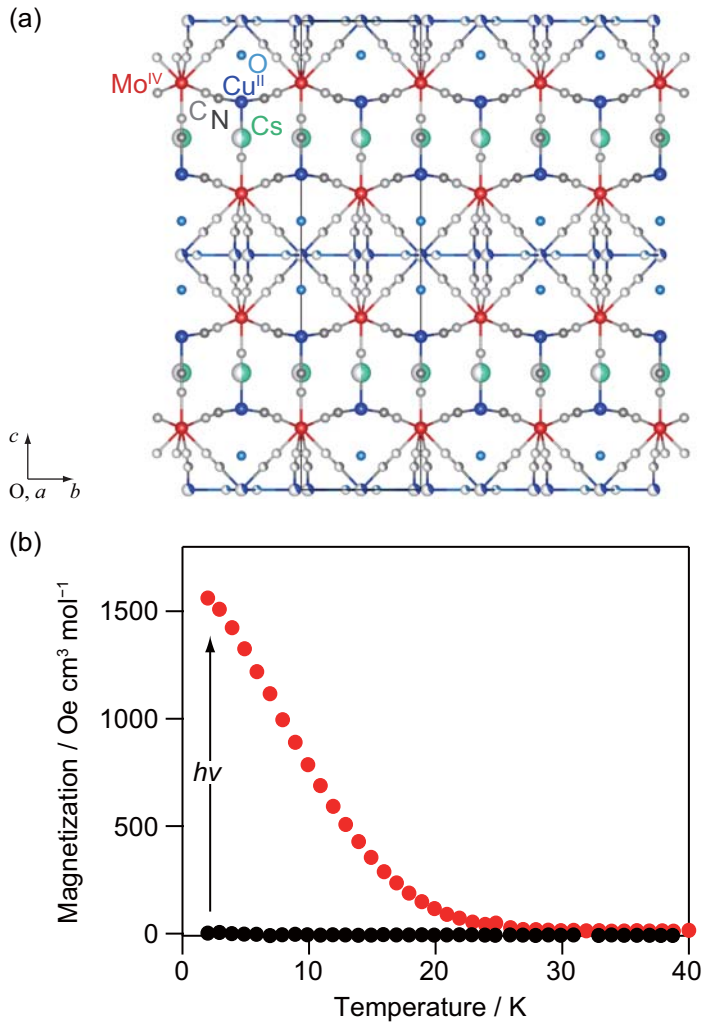

Figure 1.5. (a) Crystal structure of $Cs^{I}_{2}Cu^{II}_{7}[Mo^{IV}(CN)_{8}]_{4}\cdot 6H_{2}O$: view of the three-dimensional coordination network along the *a*-axis. Blue, red, gray, dark gray, light blue, and green spheres indicate copper, molybdenum, carbon, nitrogen, oxygen, and cesium atoms, respectively. (b) Magnetization versus temperature curves at 20 Oe. Black and red makers represents the magnetization before and after irradiation, respectively. [45]

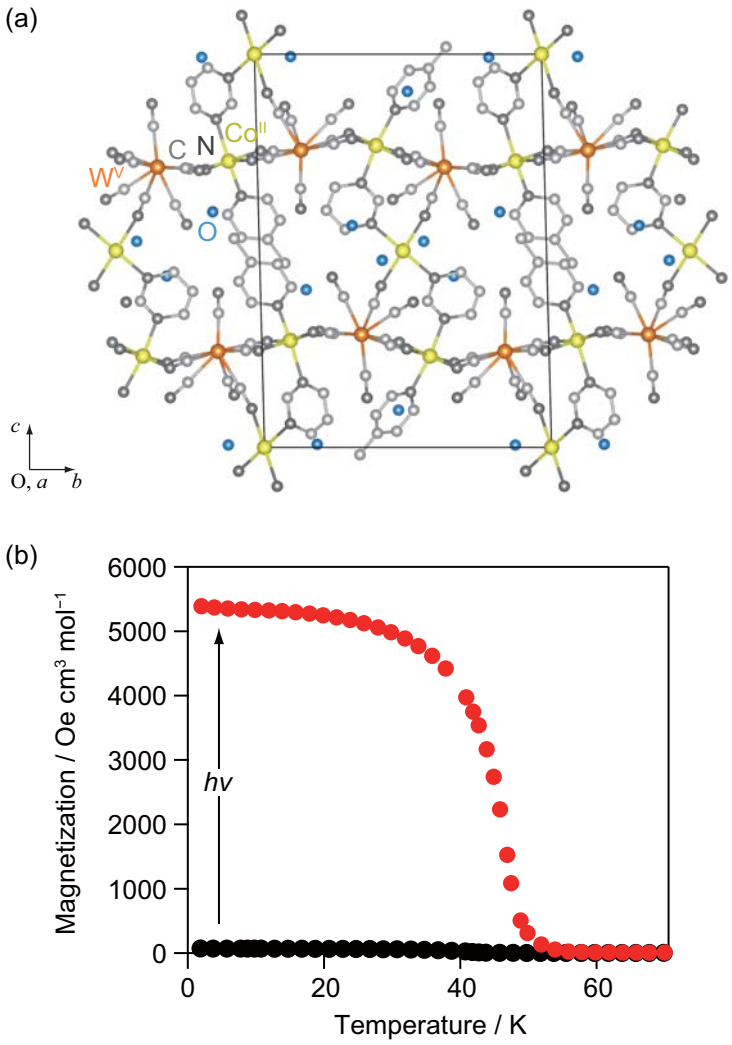

Figure 1.6. (a) Crystal structure of $[\{Co^{II}(4\text{-methylpyridine})(pyrimidine)\}_2\{Co^{II}(H_2O)_2\}\{W^V(CN)_8\}_2]\cdot 4H_2O$: view of the three-dimensional coordination network along the *a*-axis. Blue, red, gray, dark gray, and light blue spheres indicate cobalt, tungsten, carbon, nitrogen, and oxygen atoms, respectively. Hydrogen atoms are omitted for clarity. (b) Magnetization versus temperature curves at 20 Oe. Black and red makers represent the magnetization before and after irradiation, respectively. [50]

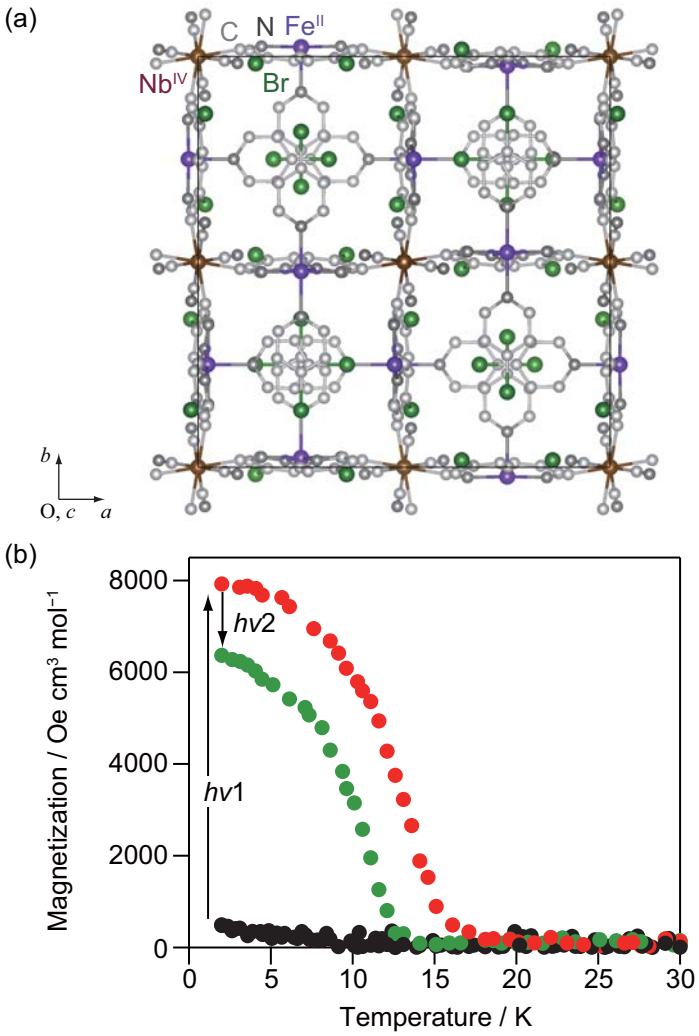

Figure 1.7. (a) Crystal structure of (+)-$Fe^{II}_2[Nb(CN)_8](4\text{-bromopyridine})_8$: view of the three-dimensional coordination network along the *c*-axis. Purple, blown, gray, dark gray, light blue, and green spheres indicate iron, niobium, carbon, nitrogen, oxygen, and bromine atoms, respectively. Hydrogen atoms are omitted for clarity. (b) Magnetization versus temperature curves at 100 Oe. Black, red, and green makers represents the magnetization before the light irradiation, after the irradiation of *hv*1, and after the irradiation of *hv*2, respectively. [52]

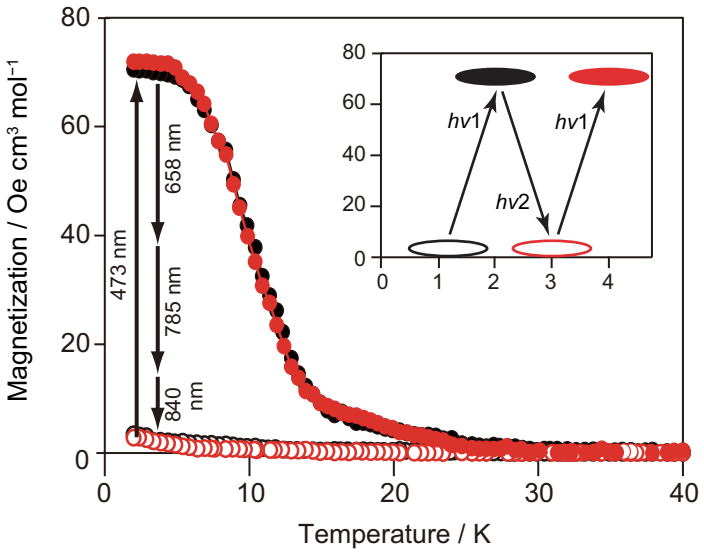

Figure 1.8. Magnetization versus temperature curves of $Cu^{II}_2[Mo^{IV}(CN)_8]_4 \cdot 8H_2O$ at 20 Oe. Black open circle, black closed circle, red open circle, and red closed circle represents the magnetization before the light irradiation, after the irradiation of 473 nm laser light (*hv*1), after the irradiation of *hv*1 and, 658, 785, and 840 nm light (*hv*2), and after the sequential irradiation of *hv*1→*hv*2→*hv*1, respectively. Inset: Magnetization change due to irradiation with *hv*1 (black closed circle), *hv*2 (red open circle), and *hv*1 (red closed circle). [46]

Reprinted with permission from S. Ohkoshi, H. Tokoro, T. Hozumi, Y. Zhang, K. Hashimoto, C. Mathoniere, I. Bord, G. Rombaut, M. Verelst, C. C. D. Moulin, F. Villain, ***J. Am. Chem. Soc.***, 128, 270 (2006). Copyright 2006, American Chemical Society.

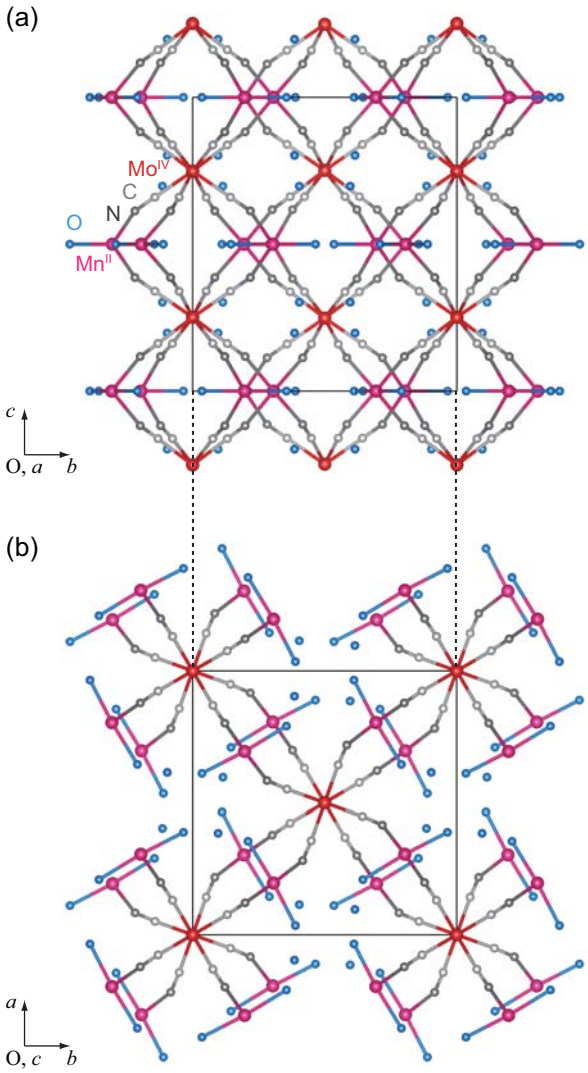

Figure 1.9. Crystal structure of $Mn^{II}[Mo^{IV}(CN)_8]\cdot 8H_2O$: views of the three-dimensional coordination network with the space group of *I*4/*m* along (a) the *a*-axis and (b) the *c*-axis. Pink, red, gray, dark gray, and light blue spheres indicate manganese, molybdenum, carbon, nitrogen, and oxygen atoms, respectively. [75]

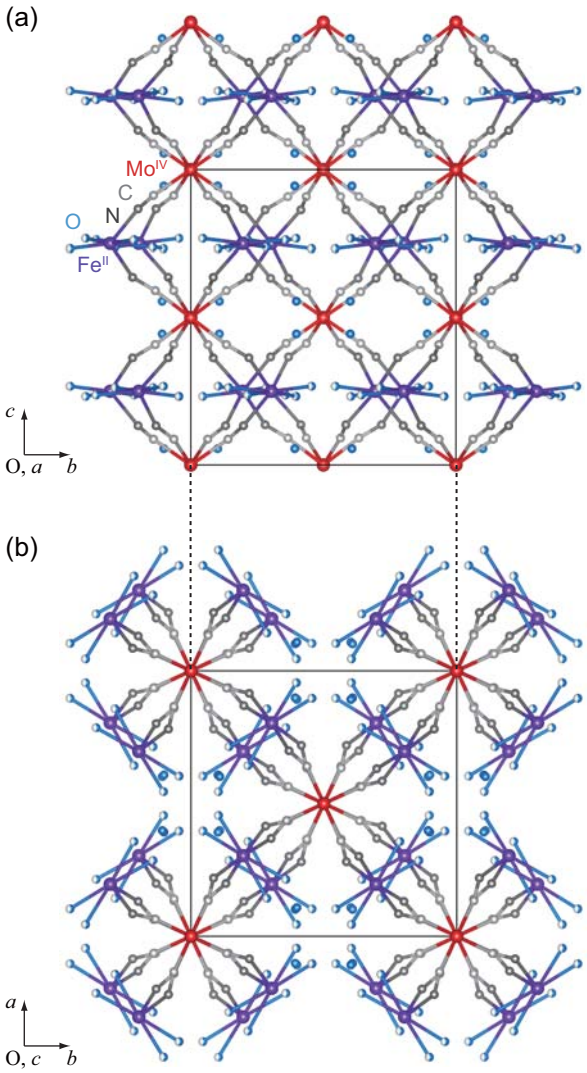

Figure 1.10. Crystal structure of $Fe^{II}[Mo^{IV}(CN)_8]\cdot 8H_2O$: views of the three-dimensional coordination network with the space group of *I*422 along (a) the *a*-axis and (b) the *c*-axis. Purple, red, gray, dark gray, and light blue spheres indicate iron, molybdenum, carbon, nitrogen, and oxygen atoms, respectively. [76]

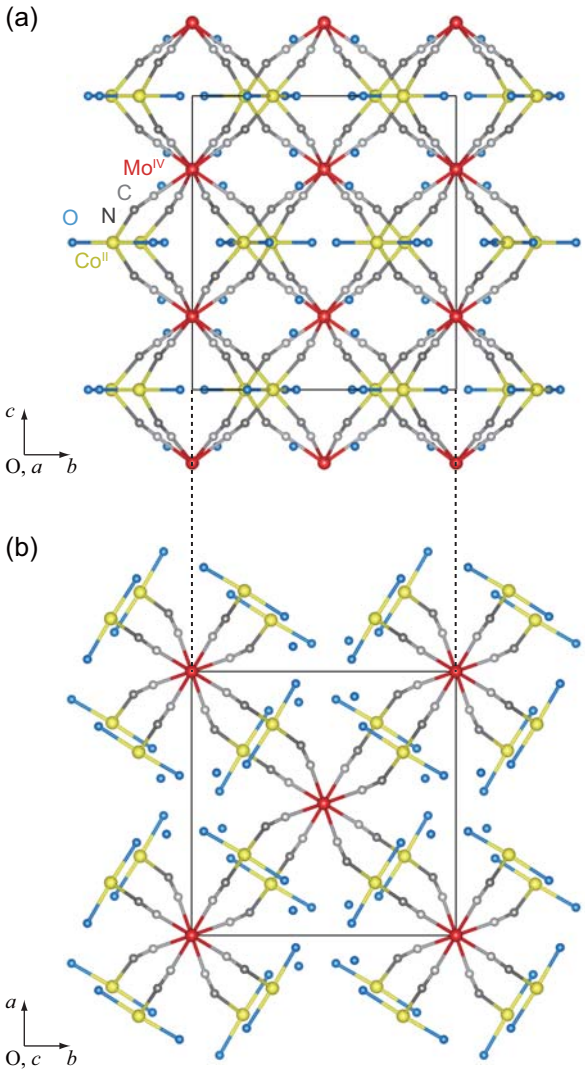

Figure 1.11. Crystal structure of $Co^{II}[Mo^{IV}(CN)_8]\cdot 8H_2O$: views of the three-dimensional coordination network with the space group of *I*4/*m* along (a) the *a*-axis and (b) the *c*-axis. Yellow, red, gray, dark gray, and light blue spheres indicate cobalt, molybdenum, carbon, nitrogen, and oxygen atoms, respectively. [77]

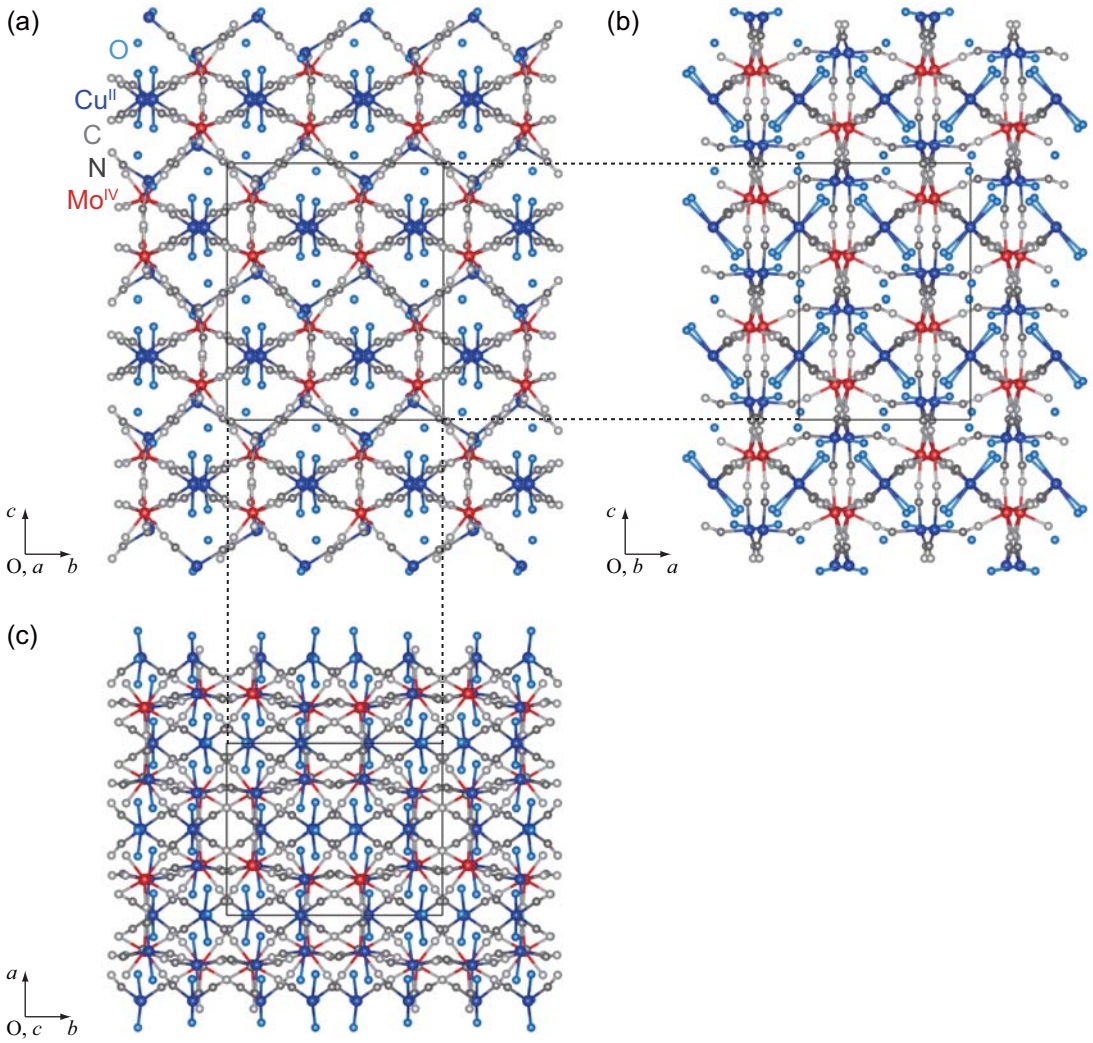

Figure 1.12. Crystal structure of $Cu^{II}[Mo^{IV}(CN)_8]\cdot 4H_2O$: views of the three-dimensional coordination network with the space group of *Pbcn* along (a) the *a*-axis, (b) the *b*-axis, and (c) the *c*-axis. Blue, red, gray, dark gray, and light blue spheres indicate copper, molybdenum, carbon, nitrogen, and oxygen atoms, respectively. [78]

Chapter 2.

Synthesis and crystal structure of copper(II) octacyanido-molybdate(IV) bimetallic assembly

---

インターネット公表に関する共著者全員の同意が得られていないため、本章については、非公開

Chapter 3.

First-principles calculations of copper(II) octacyanido-molybdate(IV) bimetallic assembly

---

インターネット公表に関する共著者全員の同意が得られていないため、本章については、非公開

Chapter 4.
Summary and prospective

In this work, I studied the visible-light induced magnetization mechanism of $Cu_2[Mo(CN)_8]\cdot nH_2O$ by first-principles calculations based on the experimentally determined crystal structure.

In chapter 2, the single crystalline form of the three-dimensional copper(II) octacyanido-molybdate(IV) $Cu_2[Mo(CN)_8]\cdot 4H_2O$ (**CuMo**) was successfully synthesized and characterized. Single crystals of **CuMo** are synthesized by a gel method with silicic acid. The single crystal X-ray diffraction analysis indicated a tetragonal crystal system, in which a three-dimensional network structure was constructed based on cyanido-bridged Cu-Mo assemblies with tetragonal crystal system. The independent structure contains one Cu center and one Mo center. The coordination geometry of the Cu center is a five-coordinated square-pyramid, and that of Mo center is an eight-coordinated square-antiprism. The Cu center is coordinated to four cyanides and one water molecule. The three-dimensional structure has a nano-porous along a-axis, where two non-coordinated water molecules per $\{Cu^{II}_2Mo^{IV}\}$ unit are placed. As a result, the overall composition is $\{[Cu^{II}(H_2O)]_2[Mo^{IV}(CN)_8]\}\cdot 2H_2O$. The framework of the structure is similar to other octacyanidomolybdate-based with 3d transition metal cations (Mn^{II}, Fe^{II}, and Co^{II}), but the number of water molecules coordinated to 3d transition metals is different.

In chapter 3, the results of first-principles calculations of **CuMo** are discussed. The first-principles band calculations using GGA + *U* method revealed the band structure and the origin of the optical transitions in the visible range. **CuMo** shows a direct transition at the Γ point with the band gap of 1.2 eV. The top of the valence band and the bottom of the conduction band are formed by a Mo^{IV} 4d-based band and a Cu^{II} 3d-based band, respectively. The optical transition calculation revealed that the absorption strength in the visible are derived from the bands mainly from Mo^{IV} 4d-orbital to those mainly from Cu^{II} 3d-orbital. This means that the visible light absorption of

CuMo is due to metal-to-metal charge transfer (MMCT) from Mo^{IV} to Cu^{II}. The result indicates that the experimental observations of the changes triggered by a visible light irradiation can be assigned to MMCT mechanism for this particular compound, and the preferred mechanism for the visible-light induced photomagnetism in our previous works is also to be based on MMCT mechanism. The charge density analysis shows that the bridging cyanide ligands facilitates the charge transfer probability, as the charge density on the nitrogen of the cyanide ligands significantly changes from the p_z orbital to the sp_x orbital. The result implies that the changes in the center and parity of the orbital allows the strong absorption behavior in the visible range. In addition, the detailed absorption strength analysis revealed that the anisotropy of the optical transition in the visible range was found for the [1 1 1] crystallographic zone axis. The [1 1 1] direction is parallel to the bridging cyanide ligands, suggesting the crucial role of the cyanide ligands in the charge transfer process.

In the previous papers [43−46], the photomagnetism in cyanide-bridged copper-molybdate bimetallic assembly is explained by a mixed valence mechanism. In this work, the first principles calculations rigidly revealed that the mechanism is the metal-to-metal charge transfer (MMCT) from Mo^{IV} to Cu^{II}. The results in this work are expected to give a design criteria for new photo-functional copper octacyanidomolybdate-based compounds and also other related photomagnetic materials.

References

[1] A. Nathanshon, P. Rochon, ***Chem. Rev.***, 102, 4139 (2002).

[2] M. Irie, ***Chem. Rev.***, 100, 1685 (2000).

[3] M. Irie, T. Fukaminato, K. Matsuda, S. Kobatake, ***Chem. Rev.***, 114, 12174 (2014).

[4] S. Decurtins, P. Gutlich, C. P. Kohler, H. Spiering, A. Hauser, ***Chem. Phys. Lett.***, 105, 1 (1984).

[5] A. Hauser, ***J. Chem. Phys.***, 94, 2741 (1991).

[6] S. Cobo, D. Ostrovskii, S. Bonhommeau, L. Vendier, G. Molnár, L. Salmon, K. Tanaka, A. Bousseksou. ***J. Am. Chem. Soc.***, 130, 9019 (2008).

[7] M. Wuttig, N. Yamada, ***Nat. Mater.***, 6, 824 (2007)

[8] S. Koshihara, Y. Tokura, T. Mitani, G. Saito, T. Koda, ***Phys. Rev. B***, 42, 6853 (1990).

[9] S. Ohkoshi, Y. Tsunobuchi, T. Matsuda, K. Hashimoto, A. Namai, F. Hakoe, H. Tokoro, ***Nat. Chem.***, 2, 539 (2010).

[10] H. Tokoro, M. Yoshikiyo, K. Imoto, A. Namai, T. Nasu, K. Nakagawa, N. Ozaki, F. Hakoe, K. Tanaka, K. Chiba, R. Makiura, K. Prassides, S. Ohkoshi, ***Nat. Comm.***, 6, 7037 (2015).

[11] O. Kahn, Molecular Magnetism, VCH, New York (1993).

[12] Gütlich, H. A. Goodwin, in Spin Crossover in Transition Metal Compounds I (eds P. Gütlich, H. A. Goodwin,) Ch.1, Springer, Berlin (2004).

[13] M. Verdaguer, A. Bleuzen, V. Marvaud, J. Vaissermann, M. Seuleiman, C. Desplanches, A. Scuiller, C. Train, R. Garde, G. Gelly, C. Lomenech, I. Rosenman, P. Veillet, C. Cartier, F. Villain, ***Coord. Chem. Rev.***, 190, 1023 (1999).

[14] S. Ohkoshi, H. Tokoro, ***Acc. Chem. Res.***, 45, 1749 (2012).

[15] J. S. Miller, ***Chem. Soc. Rev.***, 40, 3266 (2011).

[16] X.-Y. Wang, C. Avendaño, K. R. Dunbar, ***Chem. Soc. Rev.***, 40, 3213 (2011).

[17] M. Ohba, W. Kaneko, S. Kitagawa, T. Maeda, M. Mito, ***J. Am. Chem. Soc.***, 130, 4475

(2008).

[18] P. Dechambenoit, J. R. Long, ***Chem. Soc. Rev.***, 40, 3249 (2011).

[19] M. B. Robin, P. Day, Adv. Inorg. Chem. Radiochem., 10, 247 (1967).

[20] T. Matsuda, H. Tokoro, M. Shiro, K. Hashimoto, S. Ohkoshi, ***Acta Cryst. E***, 64, i11, (2008).

[21] S. Ohkoshi, T. Matsuda, S. Saito, T. Nuida, H. Tokoro, ***J. Phys. Chem. C***, 112, 13095 (2008).

[22] B. Mayoh, P. Day, ***J. Chem. Soc. Dalton Trans.***, 1483 (1976).

[23] K. Itaya, I. Uchida, V. D. Neff, ***Acc. Chem. Res.***, 162 (1986).

[24] M. Okubo, D. Asakura, Y. Mizuno, J. Kim, T. Mizokawa, T. Kudo, I. Honma, ***J. Phys. Chem. Lett.***, 1, 2063 (2010)

[25] V. M. Kämper, M. Wagner, A. Weiβ, ***Angew. Chem.***, 91, 517 (1979).

[26] S. Ohkoshi, K. Arai, Y. Sato, K. Hashimoto, ***Nat. Mat.***, 3, 857 (2004).

[27] A. Ito, M. Suenaga, K. Ono, ***J. Chem. Phys.***, 48, 3597 (1968).

[28] T. Mallah, S. Thiebaut, M. Verdaguer, P. Veillet, ***Science***, 262, 1554 (1993).

[29] S. Ferlay, T.Mallah, R. Ouahès, P. Veillet, M. Verdaguer, ***Nature***, 378, 701 (1995).

[30] S. Ohkoshi, O. Sato, T. Iyoda, A. Fujishima, K. Hashimoto, ***Inorg. Chem.***, 36, 268 (1997).

[31] S. Ohkoshi, K. Hashimoto, ***Phys. Rev. B***, 56, 11642 (1998).

[32] S. Ohkoshi, K. Hashimoto, ***J. Am. Chem. Soc.***, 121, 10591 (1999).

[33] S. Ohkoshi, H. Tokoro, T. Matsuda, H. Takahashi, H. Irie, K. Hashimoto, ***Angew. Chem. Int. Ed.***, 46, 3238 (2007).

[34] H. Tokoro, S. Ohkoshi, ***Appl. Phys. Lett.***, 93, 021906 (2008).

[35] S. Ohkoshi, K. Nakagawa, K. Tomono, K. Imoto, Y. Tsunobuchi, H. Tokoro, ***J. Am. Chem. Soc.***, 132, 6620 (2010).

[36] S. Ohkoshi, K. Hashimoto, ***Phys. Rev. B***, 60, 12820 (1999).

[37] B. Nowicka, T. Korzeniak, O. Stefańczyk, D. Pinkowicz, S. Chorazy, R. Podgajny, B. Sieklucka, ***Coord. Chem. Rev.***, 256, 1946 (2012).

[38] S. Chorazy, R. Podgajny, K. Nakabayashi, J. Stanek, M. Rams, B. Sieklucka, S. Ohkoshi, ***Angew. Chem. Int. Ed.***, 54, 5093 (2015).

[39] S. Chorazy, K. Nakabayashi, K. Imoto, J. Mlynarski, B. Sieklucka, S. Ohkoshi, ***J. Am. Chem. Soc.***, 134, 16151 (2012).

[40] K. Nakabayashi, S. Chorazy, D. Takahashi, T. Kinoshita, B. Sieklucka, S. Ohkoshi, ***Cryst. Growth Des.***, 14, 6093 (2014).

[41] K. Orisaku, K. Imoto, Y. Koide, S. Ohkoshi, ***Cryst. Growth Des.***, 13, 5267 (2013).

[42] Z. J. Zhong, H. Seino, Y. Mizobe, M. Hidai, A. Fujishima, S. Ohkoshi, K. Hashimoto, ***J. Am. Chem. Soc.***, 122, 2952 (2000).

[43] S. Ohkoshi, N. Machida, Y. Abe, Z. J. Zhong, K. Hashimoto, ***Chem. Lett.***, 312 (2001).

[44] S. Ohkoshi, N. Machida, Z. J. Zhong, K. Hashimoto, ***Synth. Met.***, 122, 523 (2001).

[45] T. Hozumi, K. Hashimoto, S. Ohkoshi, ***J. Am. Chem. Soc.***, 127, 3864 (2005).

[46] S. Ohkoshi, H. Tokoro, T. Hozumi, Y. Zhang, K. Hashimoto, C. Mathonière, I. Bord, G. Rombaut, M. Verelst, C. C. dit Moulin, F. Villain, ***J. Am. Chem. Soc.***, 128, 270 (2006).

[47] Y. Arimoto, S. Ohkoshi, Z. J. Zhong, H. Seino, Y. Mizobe, K. Hashimoto ***J. Am. Chem. Soc.***, 125, 9240 (2003).

[48] S. Ohkoshi, S. Ikeda, T. Hozumi, T. Kashiwagi, K. Hashimoto, ***J. Am. Chem. Soc.***, 128, 5320 (2006).

[49] S. Ohkoshi, Y. Hamada, T. Matsuda, Y. Tsunobuchi, H. Tokoro, ***Chem. Mater.***, 20, 3048 (2008).

[50] N. Ozaki, H. Tokoro, Y. Hamada, A. Namai, T. Matsuda, S. Kaneko, S. Ohkoshi, ***Adv. Funct. Mater.***, 22, 2089 (2012).

[51] S. Ohkoshi, K. Imoto, Y. Tsunobuchi, S. Takano, H. Tokoro, ***Nat. Chem.***, 3, 564. (2011).

[52] S. Ohkoshi, S. Takano, K. Imoto, M. Yoshikiyo, A. Namai, H. Tokoro, ***Nat. Photon.***, 8, 65 (2014).

[53] S. Ohkoshi, Y. Arimoto, T. Hozumi, H. Seino, Y. Mizobe, K. Hashimoto, ***Chem Commun.***, 22, 2772 (2003).

[54] S. Ohkoshi, Y. Tsunobuchi, H. Takahashi, T. Hozumi, M. Shiro, K. Hashimoto, ***J. Am. Chem. Soc.***, 129, 3084 (2007).

[55] Y. Tsunobuchi, W. Kosaka, T. Nuida, S. Ohkoshi, ***Cryst. Eng. Comm.***, 11, 2051 (2009).

[56] R. L. Bris, Y. Tsunobuchi, C. Mathoniere, H. Tokoro, S. Ohkoshi, N. Ould–Moussa, G. Molnar, A. Bousseksou, J. F. Letard, ***Inorg. Chem.***, 51, 2852 (2012).

[57] H. Tokoro, K. Nakagawa, K. Nakabayashi, T. Kashiwagi, K. Hashimoto, S. Ohkoshi, ***Chem. Lett.***, 38, 338 (2009).

[58] Y. Umeta, H. Tokoro, N. Ozaki, S. Ohkoshi, ***AIP Adv.***, 3, 042133 (2013).

[59] D. Rehorek, J. Salvetter, A. Hantschmann, H. Hennig, Z. Stasicka, A. Chodkowska, ***Inorg. Chim. Acta***, 37, L471 (1979).

[60] B. Sieklucka, ***Prog. React. Kinet.***, 15, 175 (1989).

[61] H. Hennig, A. Rehorek, D. Rehorek, P. Thomas, D. Bäzold, ***Inorg. Chim. Acta***, 77, L11 (1983).

[62] H. Hennig, A. Rehorek, D. Rehorek, P. Thomas, ***Inorg. Chim. Acta***, 86, 41 (1984).

[63] G. Rombaut, M. Verelst, S. Golhen, L. Ouahab, C. Mathonière, O. Kahn, ***Inorg. Chem.***, 40, 1151 (2001).

[64] J. M. Herrera, V. Marvaud, M. Verdaguer, J. Marrot, M. Kalisz, C. Mathonière, ***Angew. Chem. Int. Ed.***, 43, 5468 (2004).

[65] J. Long, L.-M. Chamoreau, C. Mathonière, V. Marvaud, ***Inorg. Chem.***, 48, 22 (2009).

[66] C. Maxim, C. Mathonière, M. Andruh, ***Dalton Trans.***, 7805 (2009).

[67] W. Zhang, H.-L. Sun, O. Sato, ***Cryst. Eng. Comm.***, 12, 4045 (2010).

[68] W. Zhang, H.-L. Sun, O. Sato, ***Dalton Trans.***, 40, 2735 (2011).

[69] F. Volatron, D. Heurtaux, L. Catala, C. Mathonière, A. Gloter, O. Stéphan, D. Repetto, M. Clemente-León, E. Coronado, T. Mallah, ***Chem. Commun.***, 47, 1985 (2011).

[70] M.-A Arrio, J. Long, C. C. dit Moulin, A. Bachschmidt, V. Marvaud, A. Rogalev, C. Mathonière, F. Wilhelm, P. Sainctavit, ***J. Phys. Chem. C***, 114, 593 (2010).

[71] S. Brossard, F. Volatron, L. Lisnard, M.-A. Arrio, L. Catala, C. Mathonière, T. Mallah, C.

C. dit Moulin, A. Rogalev, F. Wilhelm, A. Smekhova, P. Sainctavit, ***J. Am. Chem. Soc.***, 134, 222 (2012).

[72] O. Bunău, M.-A. Arrio, Ph. Sainctavit, L. Paulatto, M. Calandra, A. Juhin, V. Marvaud, C. C. dit Moulin, ***J. Phys. Chem. A***, 116, 8678 (2012).

[73] N. Bridonneau, J. Long, J.-L. Cantin, J. von Bardeleben, D. R. Talham, V. Marvaud, ***RSC Adv.***, 5, 16696 (2015).

[74] N. Bridonneau, J. Long, J.-L. Cantin, J. von Bardeleben, S. Pillet, E.-E. Bendeif, D. Aravena, E. Ruiz, V. Marvaud, ***Chem. Commun.***, 51, 8229 (2015).

[75] J. M. Herrera, P. Franz, R. Podgajny, M. Pilkington, M. Biner, S. Decurtins, H. Stoeckli-Evans, A. Neels, R. Garde, Y. Dromze, M. Julve, B. Sieklucka, K. Hashimoto, S. Ohkoshi, M. Verdaguer, ***C. R. Chimie***, 11, 1192 (2008).

[76] A. K. Sra, G. Rombaut, F. Lahitête, S. Golhen, L. Ouahab, C. Mathonière, J. V. Yakhmi, O. Kahn, ***New J. Chem.***, 24, 871 (2000).

[77] F. Tuna, S. Golhen, L. Ouahab, J.-P. Sutter, ***C. R. Chimie***, 6, 377 (2003).

[78] Y. Zhang, T. Hozumi, K. Hashimoto, S. Ohkoshi, ***Acta Cryst. E***, 63, i30 (2007).

[79] H. K. Henisch, J. Dennis, J. I. Hanoka, ***J. Phys. Chem. Solids***, 26, 493 (1965).

[80] R. E. Lisegang, ***Z. Phys. Chem.***, 88, 1 (1914).

[81] F. Bloch, ***Z. Physik***, 52, 555 (1928).

[82] R. M. Martin, Electronic Structure: Basic Theory and Practical Methods, Cambridge University Press, Cambridge (2004).

[83] L. H. Thomas, ***Proc. Cambridge Phil. Roy. Soc.***, 23, 542 548 (1927).

[84] E. Fermi, ***Rend. Accad. Naz. Lincei.***, 6, 602 (1927).

[85] P. Hohenberg, W. Kohn, ***Phys. Rev.***, 136, B864 (1964).

[86] W. Kohn, L. J. Sham, ***Phys. Rev.***, 140, A1133 (1965).

[87] J. G. Leipoldt, L. D. C. Bok, P. J. Cilliers, ***Z. Anorg. Allg. Chem.***, 409, 343 (1974).

[88] G. M. Sheldrick, ***Acta Cryst.***, A64, 112 (2008).

[89] M. Llunell, D. Casanova, J. Cirera, P. Alemany, S. Alvarez, *SHAPE, v. 2.0; Program for*

the Stereochemical Analysis of Molecular Fragments by Means of Continuous Shape Measures and Associated Tools; Departament de Química Física, Departament de Química Inorgànica, and Institut de Química Teòrica i Computacional, Universitat de Barcelona: Barcelona, Spain, 2010.

[90] D. Casanova, J. Cirera, M. Llunell, P. Alemany, D. Avnir, S. Alvarez, *J. Am. Chem. Soc.* **2004**, *126*, 1755.

[91] S. Alvarez, P. Alemany, D. Casanova, J. Cirera, M. Llunell, D. Avnir, *Coord. Chem. Rev.* **2005**, *249*, 1693.

[92] G. Kresse, J. Hafner, ***Phys. Rev. B***, 47, 558 (1993).

[93] G. Kresse, J. Hafner, ***Phys. Rev. B***, 49, 14251 (1994).

[94] G. Kresse, J. Furthmüller, ***Comput. Mat. Sci.***, 6, 15 (1996).

[95] G. Kresse, J. Furthmüller, ***Phys. Rev. B***, 54, 11169 (1996).

[96] P. E. Blöchl, ***Phys. Rev. B***, 50, 17953 (1994).

[97] G. Kresse, D. Joubert, ***Phys. Rev. B***, 59, 1758 (1999).

[98] J. P. Perdew, K. Burke, M. Ernzerhof, ***Phys. Rev. Lett***., 77, 3865 (1996).

[99] J. P. Perdew, K. Burke, M. Ernzerhof, ***Phys. Rev. Lett.***, 78, 1396 (1997).

[100] K. Monma, F. Izumi, ***J. Appl. Cryst.***, 44, 1272 (2011).

List of papers related to the thesis

(1) “Synthesis of the Single-Crystalline Form and First-Principles Calculations of Photomagnetic Copper(II) Octacyanidomolybdate(IV)”

Y. Umeta, S. Chorazy, K. Nakabayashi, S. Ohkoshi,

European Journal of Inorganic Chemistry, *in press*.

This paper corresponds to Chapter 2 and 3.

Acknowledgement

First of all, I would like to express my great gratitude to my supervisor, Prof. Shin-ichi Ohkoshi. I can conducted my work owing to the fascinating research theme and favorable environment, which he arranged. His passion towards researches, daily discussions, and suggestions inspired me. Once again I thank him for giving me opportunities to present my work in domestic and international conferences.

I am grateful to Dr. Koji Nakabayashi, Dr. Szymon Chorazy, Dr. Kenta Imoto, and Dr. Keiko Komori-Orisaku for their daily fruitful discussion and assistance. I appreciate the MERIT program for financial and encouraging my work. I acknowledge my vice-supervisor in the MERIT program, Prof. Kazushi Kanoda for significant discussion and supporting. I am also thankful to Prof. Hiroko Tokoro in Tsukuba University. I am grateful to Dr. Kosuke Nakagawa, Dr. Asuka Namai, Ms. Marie Yoshikiyo.

I am thankful to Dr. Aiko Kamitsubo for the elemental analysis of organic elements.

I am grateful to all the members of Ohkoshi laboratory, Mr. Akira Takahashi, Mr. Yasuto Miyamoto, Mr. Tomomichi Nasu, Ms. Shizuka Anan, Mr. Masaya Komine, Ms. Saori Oishi, Mr. Syunsuke Oka, Mr. Kohei Okamoto, Mr. Takuma Takeda, Mr. Yuta Maeno, Mr. Koichi Nakano, Mr. Takuro Ohno, Mr. Kouki Shiraishi, Mr. Takanobu Taniguchi, Mr. Shintaro Kawabata, Mr. Katsuhiro Tanaka. Their dedicated stances for studies were good stimulus for me.

Finally, I would like to thank to my father, mother, and brother for their understanding, support, and encouragement throughout my study.

Yoshikazu Umeta